Autophagy

ISSN: (Print) (Online) Journal homepage: https://www.tandfonline.com/loi/kaup20

Vascular smooth muscle cell-derived hydrogen sulfide promotes atherosclerotic plaque stability via TFEB (transcription factor EB)-mediated autophagy

Zhenzhen Chen, Chenxi Ouyang, Haizeng Zhang, Yuanrui Gu, Yue Deng, Congkuo Du, Changting Cui, Shuangyue Li, Wenjie Wang, Wei Kong, Jingzhou Chen, Jun Cai & Bin Geng

To cite this article: Zhenzhen Chen, Chenxi Ouyang, Haizeng Zhang, Yuanrui Gu, Yue Deng, Congkuo Du, Changting Cui, Shuangyue Li, Wenjie Wang, Wei Kong, Jingzhou Chen, Jun Cai & Bin Geng (2022): Vascular smooth muscle cell-derived hydrogen sulfide promotes atherosclerotic plaque stability via TFEB (transcription factor EB)-mediated autophagy, Autophagy, DOI: 10.1080/15548627.2022.2026097

To link to this article: https://doi.org/10.1080/15548627.2022.2026097

AUTOPHAGY
https://doi.org/10.1080/15548627.2022.2026097

Taylor & Francis
Taylor & Francis Group

RESEARCH PAPER

Vascular smooth muscle cell-derived hydrogen sulfide promotes atherosclerotic plaque stability via TFEB (transcription factor EB)-mediated autophagy

Zhenzhen Chen [a,*], Chenxi Ouyang [b,*], Haizeng Zhang [a], Yuanrui Gu [b], Yue Deng [a], Congkuo Du [c], Changting Cui [a], Shuangyue Li [a], Wenjie Wang [a], Wei Kong [d], Jingzhou Chen [a], Jun Cai [a], and Bin Geng [a]

[a]Hypertension Center, State Key Laboratory of Cardiovascular Disease, National Center for Cardiovascular Diseases, Fuwai Hospital, Chinese Academy of Medical Sciences and Peking Union Medical College, Beijing, China; [b]Department of Vascular Surgery, Fuwai Hospital, Chinese Academy of Medical Sciences and Peking Union Medical College Beijing, Beijing, China; [c]Institute of Hypoxia Medicine, Wenzhou Medical University, Wenzhou, Zhejiang, China; [d]Department of Physiology and Pathophysiology, School of Basic Medical Sciences, Peking University Health Science Center, Beijing, China

ABSTRACT

Vascular smooth muscle cells (VSMCs) contribute to plaque stability. VSMCs are also a major source of CTH (cystathionine gamma-lyase)-hydrogen sulfide (H_2S), a protective gasotransmitter in atherosclerosis. However, the role of VSMC endogenous CTH-H_2S in pathogenesis of plaque stability and the mechanism are unknown. In human carotid plaques, CTH expression in $ACTA2^+$ cells was dramatically downregulated in lesion areas in comparison to non-lesion areas. Intraplaque CTH expression was positively correlated with collagen content, whereas there was a negative correlation with $CD68^+$ and necrotic core area, resulting in a rigorous correlation with vulnerability index ($r = -0.9033$). Deletion of *Cth* in VSMCs exacerbated plaque vulnerability, and were associated with VSMC autophagy decline, all of which were rescued by H_2S donor. In ox-LDL treated VSMCs, *cth* deletion reduced collagen and heightened apoptosis association with autophagy reduction, and vice versa. For the mechanism, CTH-H_2S mediated VSMC autophagosome formation, autolysosome formation and lysosome function, in part by activation of TFEB, a master regulator for autophagy. Interference with TFEB blocked CTH-H_2S effects on VSMCs collagen and apoptosis. Next, we demonstrated that CTH-H_2S sulfhydrated TFEB at Cys212 site, facilitating its nuclear translocation, and then promoting transcription of its target genes such as *ATG9A, LAPTM5* or *LDLRAP1*. Conclusively, CTH-H_2S increases VSMC autophagy by sulfhydration and activation of TFEB, promotes collagen secretion and inhibits apoptosis, thereby attenuating atherogenesis and plaque vulnerability. CTH-H_2S may act as a warning biomarker for vulnerable plaque.

ARTICLE HISTORY
Received 24 May 2021
Revised 2 January 2022
Accepted 3 January 2022

KEYWORDS
Autophagy; cystathionine gamma lyase; hydrogen sulfide; plaque stability; transcription factor EB; vascular smooth muscle cell

Introduction

Atherosclerosis is characterized by intimal plaques and cholesterol accumulation in the arterial walls, and which is a leading cause of death in the world, because of "vulnerable" plaque rupture [1]. Vascular smooth muscle cells (VSMCs) play an essential role in atherogenesis and have been considered beneficial for plaque stability [2,3]. Inflammation and lipotoxic stimulates VSMCs phenotypic switching to secret more extracellular matrix including collagen product, which is the main source of fibrous cap [4,5]. Loss of VSMCs is involved in necrosis, apoptosis, senescence and macroautophagy/autophagy of VSMCs, leading to fibrous cap thinning, necrotic core formation and calcification [2,4]. Autophagy is an intracellular adaptive response for lysosome-mediated degradation of damaged cytosolic material. In human atherosclerotic plaque, autophagy occurs in all main cell types [6], including VSMCs [7]. VSMC autophagy associated with intracellular calcium homeostasis [8], apoptosis [9] and extracellular matrix secretion [10]. VSMC-specific deletion of *Atg7* in *apoe*-knockout mice promoted plaque development and cell death [11]. Pharmacological-induced moderate autophagy increased plaque stability by inhibition VSMC senescence [12], plaque lipid accumulation and necrotic core formation [13]. Therefore, triggering VSMC autophagy is an effective therapeutic target for vulnerable plaque.

Hydrogen sulfide (H_2S), mainly generated by CTH/CSE (cystathionine gamma-lyase) in cardiovascular tissues, is a protective gasotransmitter in atherosclerosis [14]. In an $apoe^{-/-}$ atherosclerosis mouse model, aortic CTH-H_2S content was downregulated [15]. Consistently, global *cth* knockout exacerbated atherosclerosis by elevating inflammation and oxidative stress [16]. By contrast, the H_2S donor-sodium hydrosulfide hydrate (NaHS) or GYY4137 had an anti-atherogenesis effect by inhibiting endothelial inflammation and foam cell formation [15,17,18]. VSMCs are the major source of CTH-H_2S in the arterial tissues, and VSMC CTH-H_2S content was also correlated with autophagy to reduce high glucose-induced injury [19]. Therefore, whether

CONTACT Jingzhou Chen chendragon1976@aliyun.com; Jun Cai caijun@fuwaihospital.org; Bin Geng bingeng@hsc.pku.edu.cn Hypertension Center, State Key Laboratory of Cardiovascular Disease, National Center for Cardiovascular Diseases, Fuwai Hospital, Chinese Academy of Medical Sciences and Peking Union Medical College, Beijing, China

*These authors contributed equally to this article.

Supplemental data for this article can be accessed here.

VSMC endogenous CTH-H_2S mediates plaque stability, and whether via triggering autophagy remains unknown, as does the underlying mechanism.

In the present study, we compared the CTH protein expression of atherosclerotic plaque with that of non-lesion area in patients, and correlation between relative CTH protein quantitation and the plaque stability. Using VSMC-specific *cth*-deletion mice, we investigated the role of VSMC-derived CTH-H_2S in plaque stability, and then addressing on TFEB (master regulator of autophagy) sulfhydration to clarify the underlying mechanism.

Results

CTH protein expression in ACTA2-positive cells positively correlated with plaque stability

To clarify the correlation between VMSC-derived CTH-H_2S with plaque stability, we collected human plaque's slices, then performed the CTH, ACTA2/α-SMA immunofluorescence staining, CD68 histochemical and Masson staining. Here, we demonstrated that CTH protein level in ACTA2-positive cells of plaque dramatically decreased comparison to the self-non-lesion region (Figure 1A). Consistently, the downregulation of CTH in $ACTA2^+$ cells also confirmed in aortic root plaque of atherosclerotic mice (Figure S1A). In cultured human aortic smooth muscle cells (HASMCs), oxidized low-density lipoprotein (ox-LDL) also decreased *CTH* mRNA (Figure S1B) and protein expression (Figure S1C) in a dose-dependent manner. In line with *CTH* downregulation, ox-LDL (150 μg/ml) lowered endogenous H_2S generation by H_2S-fluorescence probe (mito-HS) tracking (Figure S1D). Therefore, these data highlighted VSMC endogenous CTH-H_2S downregulation associated with atherogenesis.

More intriguing, we confirmed that CTH protein expression dramatically decreased in vulnerable plaque comparison to stable plaque (characterized as small percentage of $CD68^+$ area, low necrotic core area, high percentage of $ACTA2^+$ area and great collagen volume fraction) (Figure 1B). Pearson correlation analysis showed intraplaque CTH protein level positively correlated with $ACTA2^+$ area (Figure 1C) and collagen volume fraction (Figure 1D), whereas negatively correlated with $CD68^+$ area (Figure 1E) and necrotic core area (Figure 1F). Surprisingly, intraplaque CTH level showed high coefficient of association with vulnerability index (counted by [($CD68^+$ area + necrotic core area)/($ACTA2^+$ area + collagen volume)]; $r = -0.9033$; Figure 1G). Taken together, these data suggested that intraplaque CTH expression greatly associated with plaque stability in patients.

VSMC-specific cth *deletion exacerbated plaque progression and vulnerability*

To clarify the pathophysiological relevance of VSMC endogenous CTH-H_2S in plaque stability, we generated VSMC-specific *cth* knockout mice ($cth^{SMC-/-}$) by loxp-Cre system (Figure S2A). Identification the homozygote mice, we cultured primary VSMCs and confirmed *cth* deletion (Figure S2B-C), and which lost about 75.7% H_2S generation (Figure S2D). By PCSK9 overexpression and Paigen diet feeding, we generated atherosclerosis mouse model association with elevation of plasma PCSK9 (Figure S2E). En-face Oil Red O staining showed that aortic plaques increased about 76% (including 78% in aorta arch, 79.2%in thoracic aorta (TA) and 87.3% in abdominal aorta (AA), respectively) in $cth^{SMC-/-}$ mice comparison to $Cth^{flox/flox}$ mice (Figure 2A–B and Figure S2F). Consistently, aortic root plaque area also increased about 58% in $cth^{SMC-/-}$ mice (52.00 ± 12.38% vs 32.90 ± 11.62%, Figure 2C). However, there were no statistical difference in the plasma lipid profiles (total triglyceride, total cholesterol, LDL and HDL cholesterol) (Figure S2G). All these phenotyping changes were partly rescued by supplementation H_2S donor-NaHS (20 mg/kg/day). Thus, the loss of function experiments first clarified that VSMC derived CTH-H_2S system involved in pathogenesis of atherosclerotic plaque.

To investigate the deletion of *Cth* in VSMCs in plaque stability, the necrotic core, Masson staining for fibrous content, CD68 and ACTA2 immunohistochemical staining were performed. In line with plaque size increasing, *Cth* deficiency in VSMCs also heightened the intraplaque necrotic core area about 52.8% (32.60 ± 6.09 vs 21.33 ± 8.63, Figure 2D), $CD68^+$ area about 47.8% (23.35 ± 5.17 vs 15.80 ± 3.69), but reduced collagen volume fraction about 31% (69.00 ± 23.5 vs 100 ± 21.1) (Figure 2E), resulting in elevation the vulnerability index about 39.7% (25.93 ± 6.97 vs 18.56 ± 7.43) (Figure 2F). All these vulnerable plaque phenotypes were greatly attenuated by NaHS supplementation (Figure 2D–F), furthermore confirmation the VSMC-derived CTH-H_2S essential modulation in plaque stability.

Cth *deficiency reduced plaque stability association with VSMC autophagy decline.*

Moderate VSMC autophagy is benefit for plaque stability. To investigate whether the VMSC *Cth* deficiency-induced vulnerable plaque is due to autophagy reduction, we first measured the autophagy marker-LC3 expression in the plaque. In patient's plaque, LC3 and ACTA2 double-positive cells dramatically reduced about 68.12%, comparison to non-lesion area (Figure 3A). The intraplaque autophagy declining also confirmed in ACTA2-positive cells of mouse model (Figure 3B). In $cth^{SMC-/-}$ mice, intraplaque autophagy in ACTA2-positive cells was lower than that of $Cth^{flox/flox}$ mice (LC3 fluorescence staining reduction about 76.74%, Figure 3C); observation of autophagosomes by transmission electron microscopy also confirmed it (Figure S3A), and all of which was partly rescued by NaHS (Figure 3C).

For confirmation, we cultured HASMCs, and evaluation the autophagy markers (*ATG5, BECN1, LAMP1* and *TFEB*) mRNA expression under ox-LDL stimulation (Figure S3B). According to the dose-dependent response, we selected ox-LDL (150 μg/ml) as a stimulator. What is more, *cth* deletion reduced autophagy marker genes mRNA expression (Figure S3C). Indeed, ox-LDL induced HASMC phage-like phenotype (lipid-deposition), and which was lowered by H_2S donor, but aggravated by *cth* knockout or its inhibitor (PPG) (Figure 4A). VSMC apoptosis and collagen secretion are essential for plaque stability. Therefore, we firstly demonstrated that ox-LDL

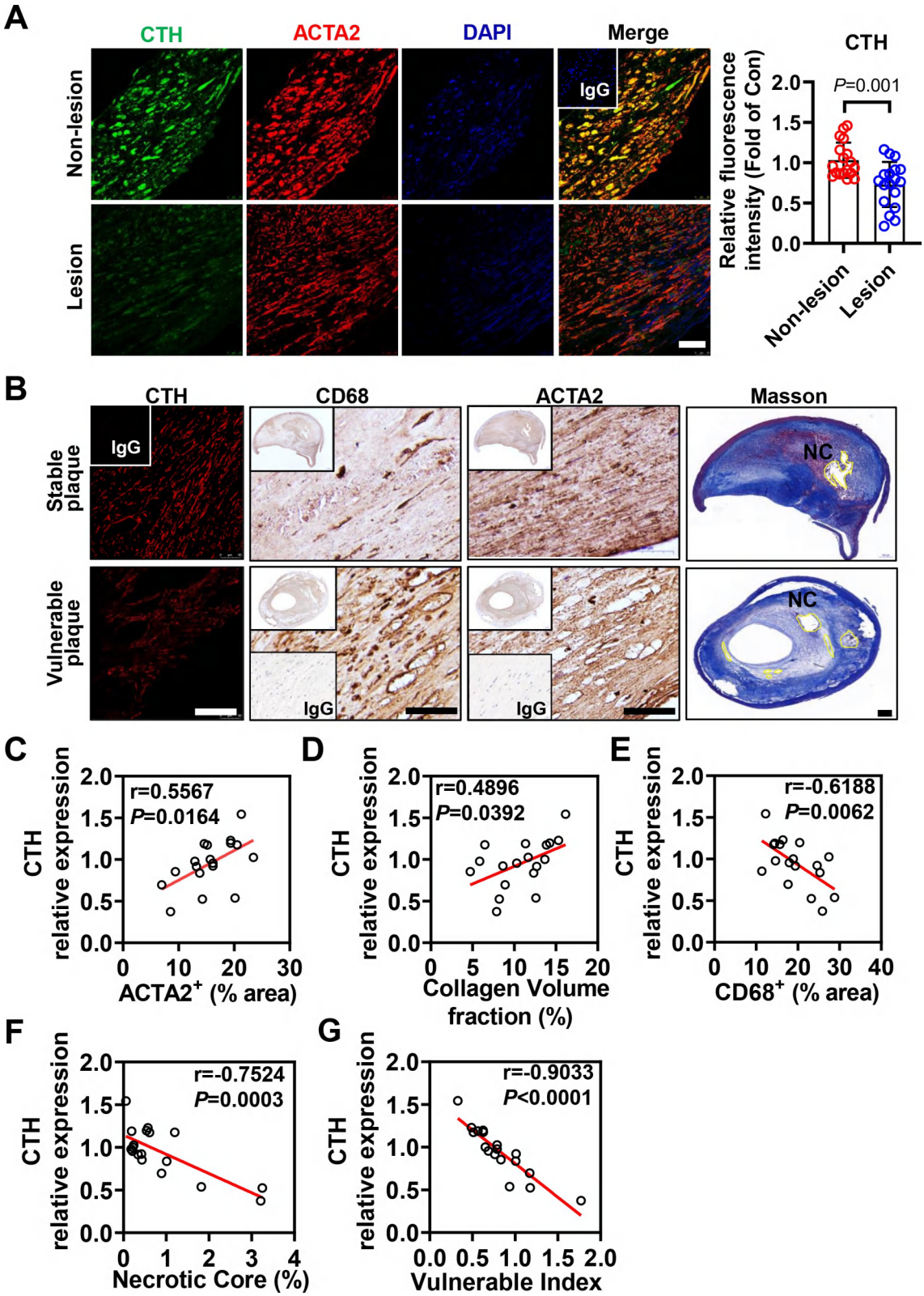

Figure 1. Patient's intraplaque CTH expression negatively correlated with plaque vulnerability. Immunofluorescent staining for CTH (green) and ACTA2 (red) in non-lesion area and lesion area of patient's carotid plaques (A), IgG as negative control. Scale bar: 50 μm. Immunofluorescent staining of CTH, immunohistochemical staining of CD68, ACTA2 and Masson staining in stable plaque and vulnerable plaque of human (B), the yellow continuous line indicates the area of necrotic core, NC: necrotic core. IgG as negative control. Scale bar from left to right: 50 μm, 50 μm, 50 μm and 500 μm. Pearson correlations between CTH expression and ACTA2 (% area) (C), collagen volume fraction (D), CD68 (% area) (E), necrotic core (% area) (F) and vulnerable index (G). Vulnerable index was counted by ($CD68^+$ area + necrotic core area)/($ACTA2^+$ area + collagen volume). N = 18/group.

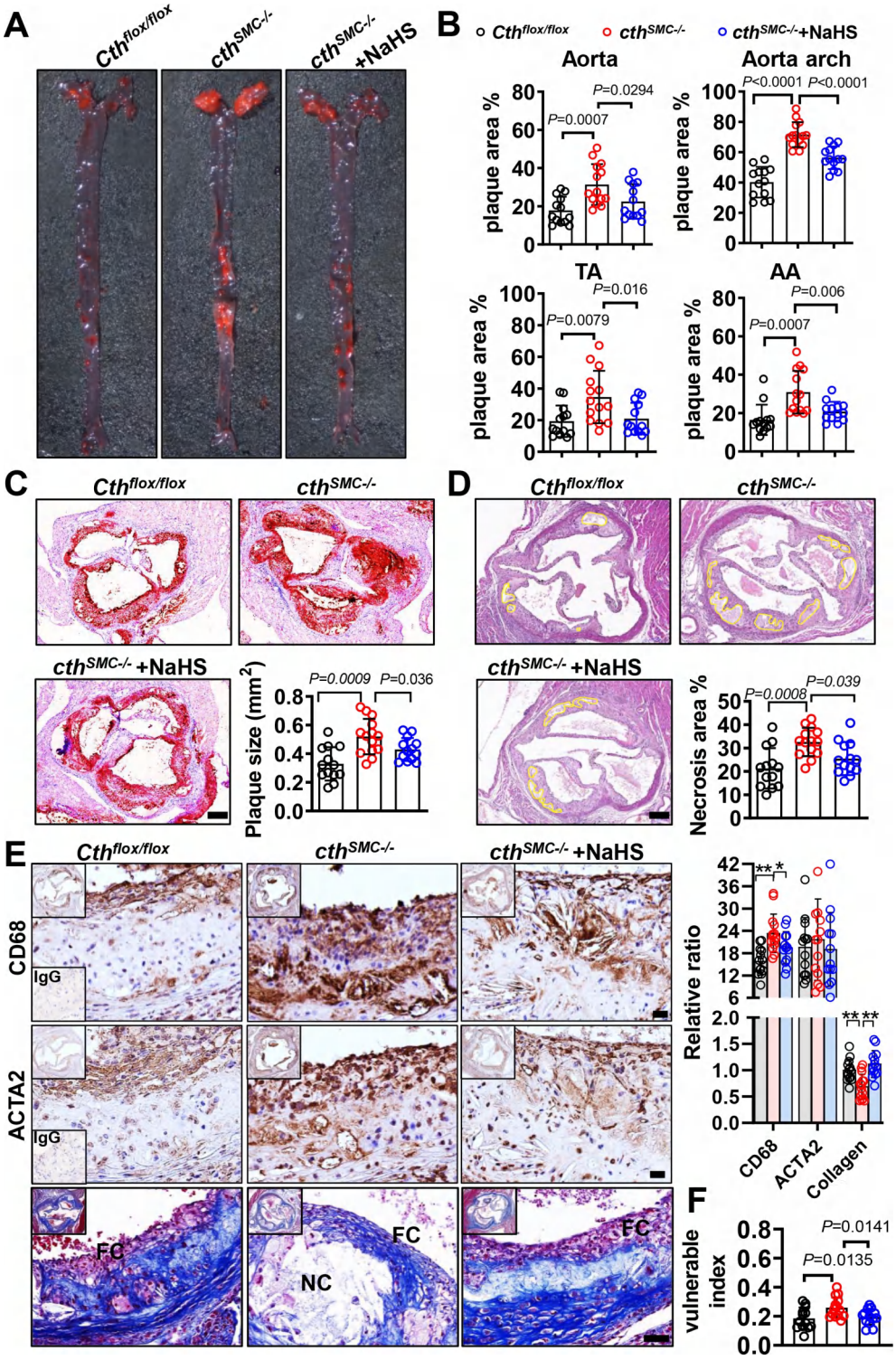

Figure 2. VSMC-specific *cth* deletion exacerbated plaque vulnerability. Using loxp-cre recombinase system, we generated a SMC-specific *cth* knockout mouse. Atherosclerosis mouse model was generated using PCSK9 overexpression in liver by injection adeno-associated virus rAAV8-D377Y-mPCSK9 then feeding Paigen diet for 16 weeks. While sacrifice, aortic en face Oil-red O staining was performed (A), and plaque area in different location was presented as a percentage of total area. AA: abdominal aorta; TA: thoracic aorta (B). Plaque size in aortic root was also evaluated by Oil-red O staining, Scale bar: 200 μm (C). The yellow line showed the size of necrotic core of aortic root plaque by H&E staining, Scale bar: 200 μm (D). In aortic root plaque, immunohistochemical staining CD68 and ACTA2 (IgG as negative control), Masson staining for collagen fraction. FC: fibrous cap; NC: necrotic core. Scale bar: 50 μm; *P < 0.05; **P < 0.01 (E). The vulnerable index changes in aortic root plaque (F). In this figure, black circle presented $Cth^{flox/flox}$ group; red circle presented $cth^{SMC-/-}$ group; blue circle present $cth^{SMC-/-}$+NaHS group. $Cth^{flox/flox}$ group: N = 13; $cth^{SMC-/-}$ group: N = 14; $cth^{SMC-/-}$+NaHS group: N = 13.

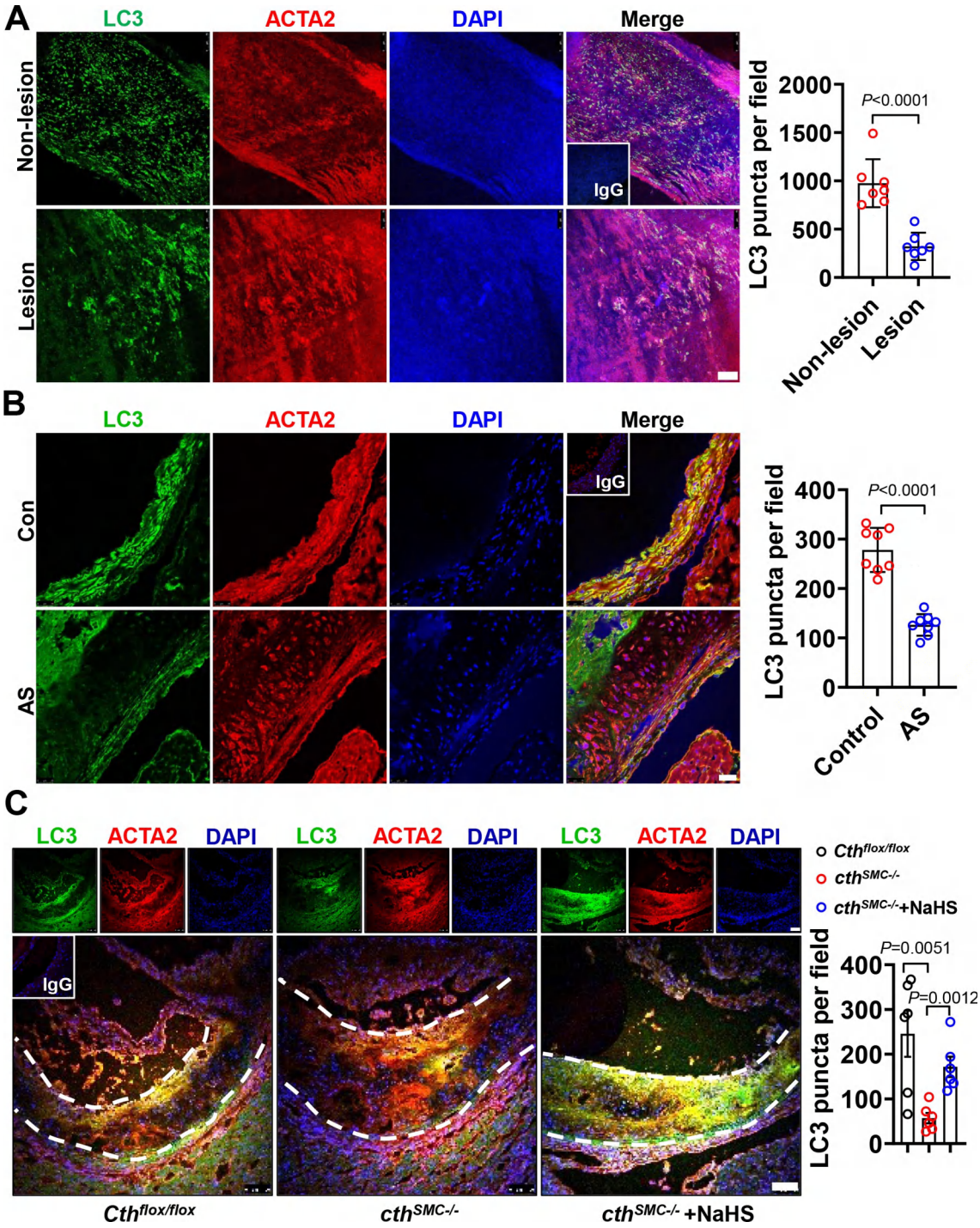

Figure 3. Autophagy changes in intraplaque ACTA2 cells of patients and mouse model. LC3 immunofluorescent staining (green) was used for evaluation autophagy, ACTA2 (red) as reference. Nuclei stained by DAPI. The carotid plaque (lesion) and non-plaque area (non-lesion) of patients, scale bar: 75 μm, N = 7 (A). normal and atherosclerotic plaque of aortic root of mice, scale bar: 25 μm, N = 8 (B). Intraplaque autophagy changes in *Cth*$^{flox/flox}$, *cth*$^{SMC-/-}$ and *cth*$^{SMC-/-}$+NaHS groups, scale bar: 25 μm, N = 6 (C). All IgG as negative controls.

heightened the HASMC apoptosis beyond 2 folds, and which were attenuated by NaHS, and aggravated by PPG (Figure 4B). Deletion of *Cth* per se did not induce, but increase ox-LDL-induced VSMC apoptosis (Figure 4C). In line with VSMC apoptosis, ox-LDL also decreased COL1 (collagen, type I) expression, and which was also partly rescued by NaHS but aggravated by PPG (Figure 4D and Figure S4A). Accordingly, *cth* knockout also enlarged COL1 expression declining in basal and ox-LDL stimulated condition (Figure 4E and Figure S4B). Collectively, these in vitro data indicated that VSMC endogenous CTH-H_2S contributed to plaque stability by modulation VMSC apoptosis and collagen secretion.

In keeping with VSMC apoptosis and collagen secretion changes, LAMP1 and LC3-II:LC3-I also declined by ox-LDL, and which were reversed by NaHS or *Cth* overexpression, but aggravated by knockdown *Cth* (Figure 4F–H and Figure S4C-H). Using GFP-mRFP-LC3 adenovirus to track the

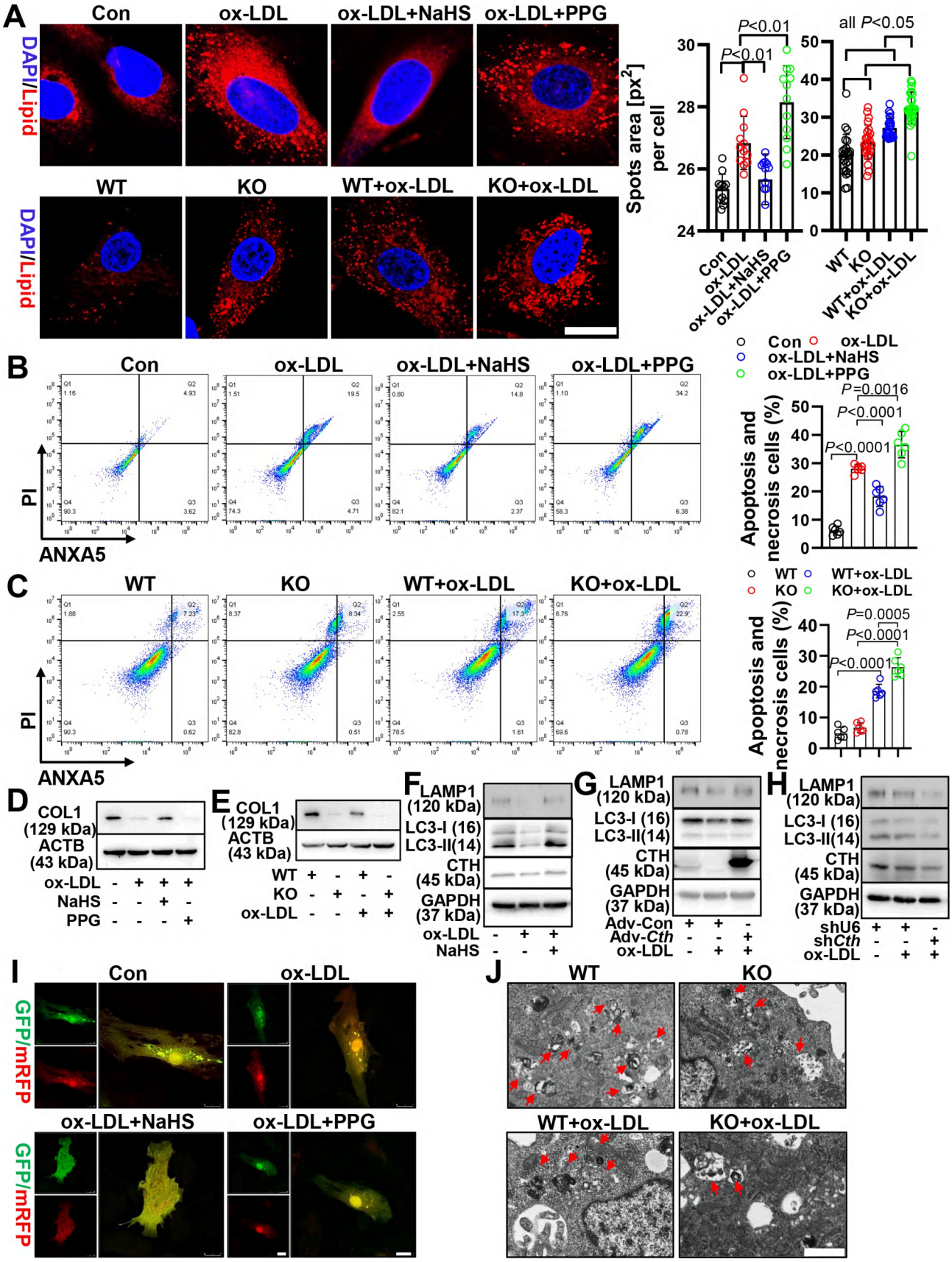

Figure 4. CTH-H_2S-modulated VSMC apoptosis, collagen secretion and phage-like phenotype associated with autophagy. Exposed to ox-LDL (150 μg/ml) for 24 h, the effect of H_2S donor NaHS (100 μM, 2 h) and CTH inhibitor PPG (100 μM, 24 h) on lipid droplet accumulation in HAMSCs (the upper panel) (N = 12); in isolated mouse VSMCs, the effect of *cth* knockout on lipid droplet accumulation both with and without ox-LDL (150 μg/ml, 24 h) in contrast with WT VSMCs (the lower panel) (N = 24). scale bar: 25 μm (A). ox-LDL induced apoptosis was analyzed by flow cytometry when pharmacological interference CTH-H_2S in HASMCs (N = 6) (B), or *cth* knockout in mouse primary VSMCs (N = 6) (C). ox-LDL impaired VSMC COL1 expression was measured by Western blot in HASMCs (D) or *Cth*-deficient VSMCs (E). Autophagy makers-LAMP1, LC3-I:LC3-II protein expression were assayed after NaHS treatment (F), *Cth* overexpression (G) and *Cth* knockdown (H) response to ox-LDL. mRFP-GFP-LC3 adenovirus were transfected to monitor autophagy flux in HASMCs while pharmacological interference CTH-H_2S. Yellow puncta presented autophagosomes numbers, red puncta presented autolysosomes formation, scale bar: 25 μm (I). Transmission electron microscope showed the autophagosomes in wild type or *cth* knockout VSMCs response to ox-LDL (150 μg/ml, 24 h) stimulation, red arrows indicate autophagosome, scale bar: 1 μm (J).

autophagy flux, we demonstrated that NaHS reversed but PPG exacerbated ox-LDL induced autophagy flux lowering (Figure 4I and Figure S5A). In comparison to wild-type VSMCs, deletion of *Cth* also exacerbated the ox-LDL-induced lipid storage (Figure S5B), autophagy flux inhibition (Figure S5C) and autophagosome decline (Figure 4J and Figure S5D-E). On the contrary, the phenotypes of lipid deposition and autophagy inhibition in *cth* knockout VSMCs were partly rescued by NaHS (Figure S5B-C). The above results suggested that CTH-H_2S mediating VSMC apoptosis and collagen secretion in part linking with VSMC autophagy.

CTH-H_2S mediated autophagosome, autolysosome formation and lysosome function.

Autophagy is a dynamic process including phagophore, autophagosome formation, autolysosome formation and lysosome clearance. To investigate the potential target of CTH-H_2S on autophagy, 3-methyladenine (3-MA)-a selective autophagosome formation inhibitor, and chloroquine (CQ)-a autophagosome-lysosome fusion inhibitor were used. As Figure 5A showed, 3-MA significant inhibited, whereas CQ aggravated *Cth* overexpression-induced elevation of LC3-II:LC3-I (Figure 5A and Figure S6A). The effect was further confirmed by tracking autophagy flux (Figure 5B). When there was deletion of *Cth*, 3-MA aggravated LC3-II:LC3-I reduction but CQ promoted LC3-II:LC3-I accumulation (Figure 5C and Figure S6B). The autophagy flux also confirmed it (Figure 5D). These findings suggested CTH not only increased autophagosomes formation but further promoted autophagosome-lysosome fusion during autophagy procession.

Lysosome function as cleaning the intracellular waste to guarantee the cell viability. By LAMP1 immunofluorescence staining (Figure 5E and Figure S6C) and LysoTracker Red staining (Figure 5F and Figure S6D), we found that ox-LDL reduced lysosome numbers. *cth* deletion exacerbated lysosome reduction and inhibited its maturation (characterized as its distribution from perinucleus to cytoplasm). An acidic environment in lysosome is required to maintain its function. Using LysoSensor to track the pH values of lysosomes, we demonstrated that NaHS (4.69 vs 5.36) can effectively block the elevation of pH value by ox-LDL (5.36 vs 4.76; Figure 5G). In contrast, CTH inhibitor-PPG (5.99 vs 5.36; Figure 5G) or *cth* deletion (6.06 vs 5.65; Figure 5H) heightened the pH value of lysosome. Therefore, CTH-H_2S deficiency impaired lysosome biogenesis and biological function. These results indicated that autophagosome, autolysosome and lysosome function involved in the regulation of CTH-H_2S on VSMC autophagy.

CTH-H_2S modulated VSMC autophagy by sulfhydrating and activating TFEB.

CTH-H_2S modulated most processes of VSMC autophagy, which are controlled by a master transcription factor, TFEB (transcription factor EB). This also led us to investigate whether CTH-H_2S regulates TFEB. In keeping with alterations of autophagy, intraplaque TFEB protein expression and its nuclear translocation were downregulated in ACTA2-positive cells of $cth^{SMC-/-}$ mice, and which was partly rescued by NaHS (Figure 6A). In vitro, NaHS also rescued the ox-LDL -reduced TFEB activity in *Cth* deficient VSMCs (Figure S7A). In HASMCs, genomic modification by overexpression or knockout of *Cth* (Figure S7B), or pharmacological interference by NaHS or PPG confirmed the CTH-H_2S promoting TFEB nuclear translocation (Figure 6B and Figure S7C-D). Next, we knocked down *TFEB* using siRNA (Figure S7E-G) and overexpress *TFEB* using plasmid (Figure S7H-J). *TFEB* knockdown blocked the NaHS protection on lipid deposition, autophagy flux (Figure 6C and Figure S7K-L), autophagy markers, COL1 expression (Figure 6D and Figure S7M) and cell apoptosis (Figure 6E); vice versa, overexpression *TFEB* attenuated the autophagy changes, COL1 expression and cell apoptosis by PPG (Figure 6F–H and Figure S7N-O). These data indicated that TFEB contributed to the regulation of CTH-H_2S on VSMC autophagy, thereby collagen secretion and apoptosis.

The post-translational modification of TFEB such as phosphorylation, modulates TFEB activity. To investigate the mechanism of CTH-H_2S action, we detected S-sulfhydration (a specific chemical modification by H_2S at cysteine residue) of TFEB. By blast, *TFEB* contained a conserved cysteine residue in helix-loop-helix domain (Figure S8A). Next, we confirmed the H_2S donor sulfhydrates TFEB (human) at the cys212 site (Figure 7A). Association with sulfhydration, TFEB nuclear translocation increased, and which was blocked by DTT (sulfhydration remover) (Figure 7B). Overexpression *Cth* increased, but *cth* knockout lowered TFEB sulfhydration (Figure 7C) and its nuclear translocation (Figure 7D), suggesting this chemical modification dependent on CTH. Mutation cysteine into serine at 212 site, abolished TFEB sulfhydration (Figure 7E), and which also blocked the H_2S effect on TFEB nuclear translocation (Figure 7F). Taken together, these results suggested that H_2S sulfhydrated TFEB to facilitate TFEB activity.

TFEB sulfhydration regulated autophagy, lysosome biogenesis and lipid metabolism-related gene transcription

To address whether the TFEB sulfhydration promoted its functional translocation and the precise target genes, we performed chromatin immunoprecipitation followed by high-throughput sequencing (ChIP-Seq) in *cth*-deleted VSMCs or C212S mutation of HEK-293 cells. By clustering *TFEB* occupied peaks within ± 3.0 kb from the center of transcription start sites (TSS), removing TFEB sulfhydration (C212S mutation) markedly restrained *TFEB* occupancy genes compared with wild type (Figure 8A); Whereas *Cth* deficiency slightly increased *TFEB* occupancy genes (Figure 8B). Then we identified 20,381 specific peaks in wild type TFEB group comparison to C212S mutation TFEB; and 14,195 specific peaks in wild type primary mouse VSMCs comparison to *cth* deletion VSMCs. By cross-analysis these peaks and corresponding genes, total 3,326 sufhydrated-TFEB modulated genes were identified (Figure 8C). Gene ontology (GO) analysis showed

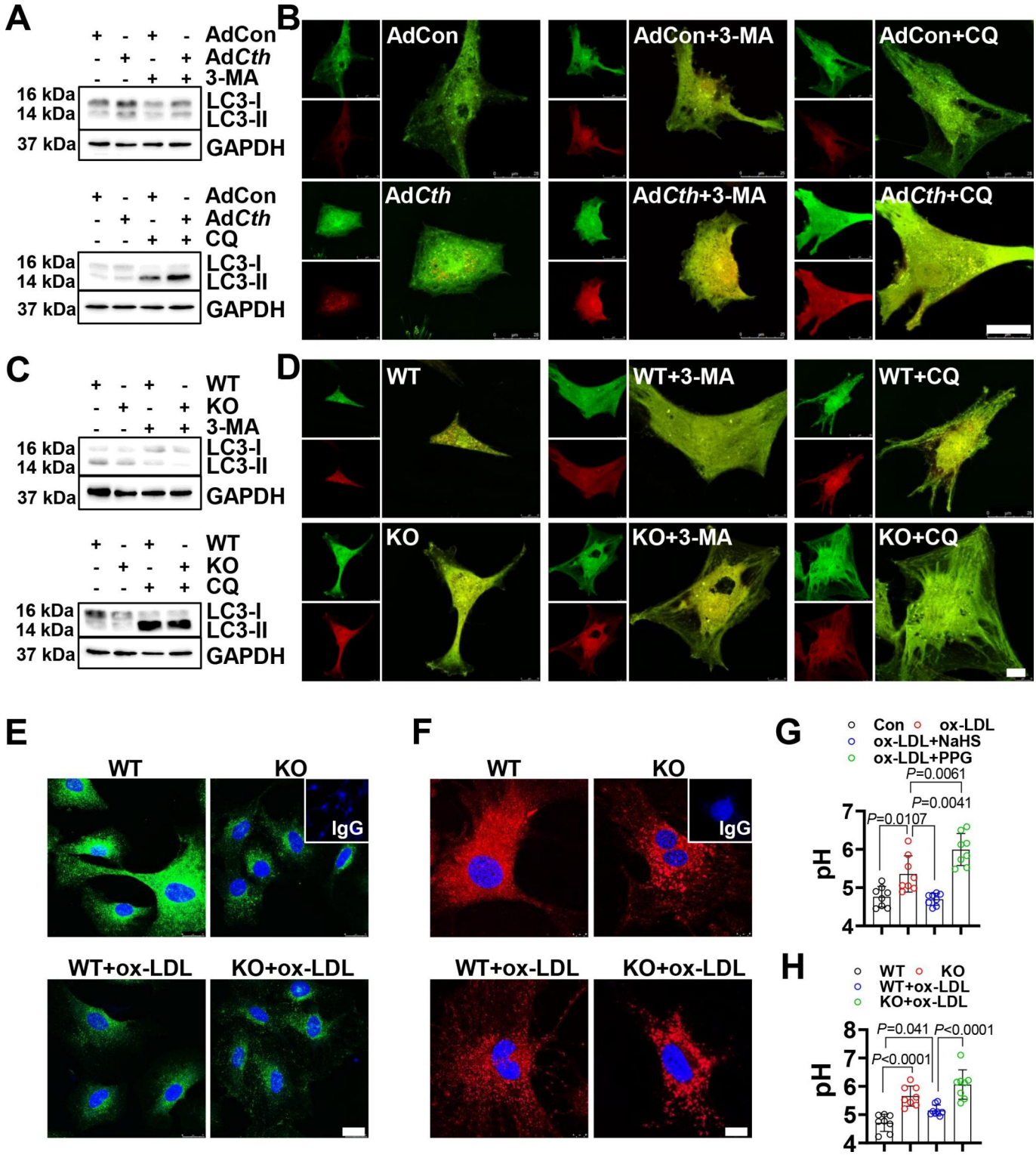

Figure 5. CTH-H_2S regulated autophagosome, autolysosome formation and lysosome function. 3-methyladenine (3-MA)-a selective autophagosome formation inhibitor, and chloroquine (CQ)-a autophagosome-lysosome fusion inhibitor were used for blocking autophagosome or autolysosome formation. After Ad*Cth* transfection for 24 h, HASMCs were pre-treated with 5 mM 3-MA for 1 h or treated with 200 μM CQ for 2 h. 3-MA blocking and CQ heightening the overexpressed CTH-induced LC3 protein accumulation (A) and autophagy flux elevation, scale bar: 25 μm (B). Effect of 3-MA and CQ on *cth*-deletion induced LC3 protein reduction (C) and autophagy flux blocking (D), scale bar: 10 μm. After ox-LDL (150 μg/ml, 24 h) treatment in primary mouse VSMCs, LAMP1 immunofluorescence staining (E), scale bar: 25 μm; or LysoTracker Red showed the numbers and location of lysosomes in VSMCs, scale bar: 10 μm (F). IgG as negative control. HASMCs (N = 8) (G) or mouse primary VSMCs (N = 8) (H) were labeled with LysoSensor, pH values were calculated by pH standard calibration while pharmacological or genomic modification CTH-H_2S.

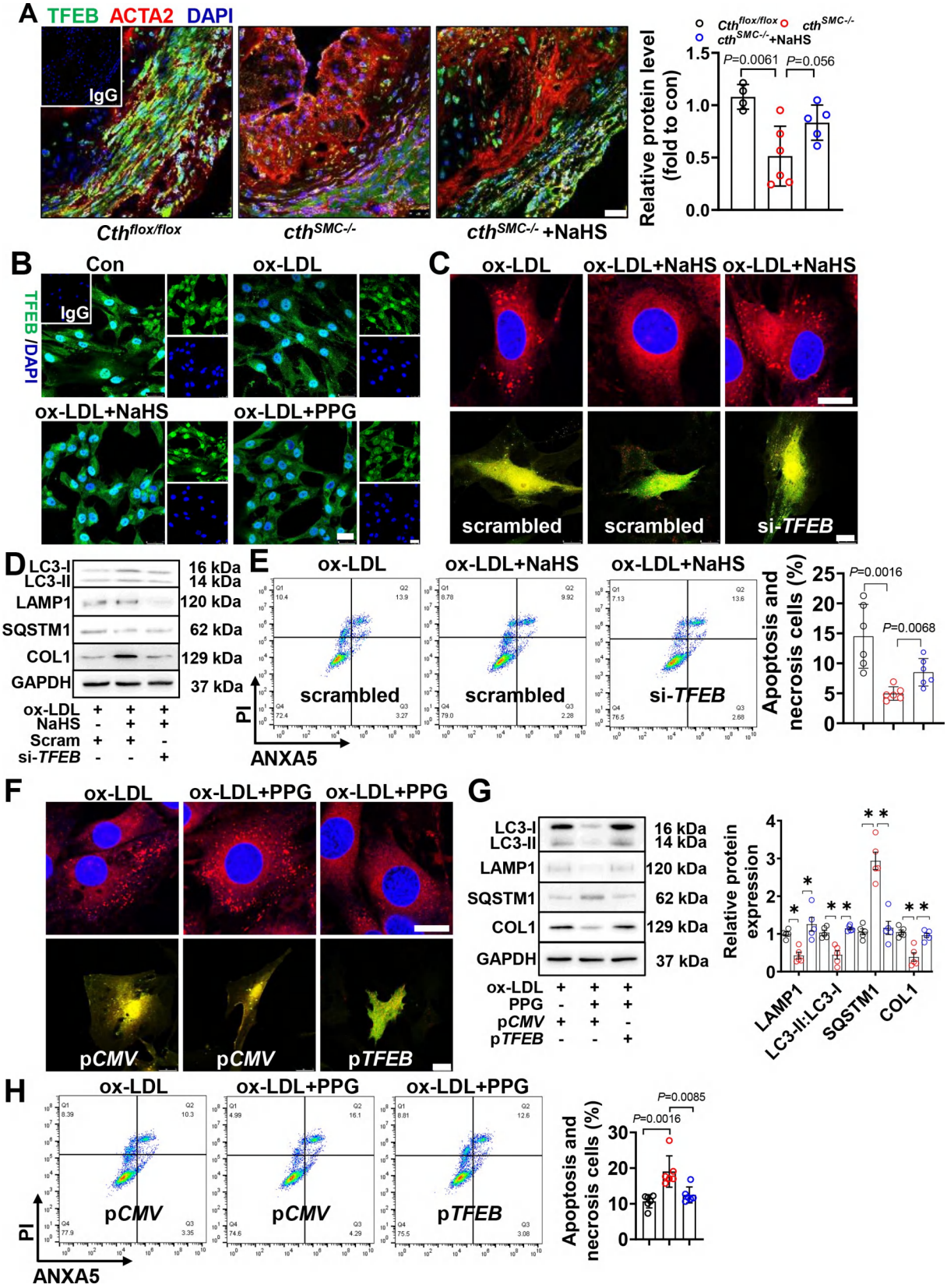

Figure 6. CTH-H_2S regulated VSMC autophagy by activating TFEB. TFEB immunofluorescence staining in intraplaque ACTA2-positive cells of *Cth*$^{flox/flox}$ (N = 4), *cth*$^{SMC-/-}$ (N = 6) and *cth*$^{SMC-/-}$ +NaHS mice (N = 5) (A). IgG as negative control. Exposed to ox-LDL (150 μg/ml) for 24 h, the effect of H_2S donor NaHS (100 μM, 2 h) and CTH inhibitor PPG (100 μM, 24 h) on TFEB expression and nuclear translocation in ox-LDL-stimulated HASMCs (B). IgG as negative control. In HASMCs, Knockdown *TFEB* by siRNA transfection (100 nM, 24 h) effects on NaHS (100 μM, 2 h) modulating VSMC phage-like phenotype and autophagy flux changes (C), COL1 and autophagy markers expression (D), and VSMC apoptosis (N = 6) (E). On the contrary, overexpressed *TFEB* by plasmid transfection (2 μg, 24 h) partly rescued PPG-induced (100 μM, 24 h) phage-like phenotype, autophagy flux decrease (F), COL1 and autophagy markers expression decrease (N = 5) (G), and VSMC apoptosis increase (N = 6) (H). *$P < 0.05$, ** $P < 0.01$. All scale bar: 25 μm.

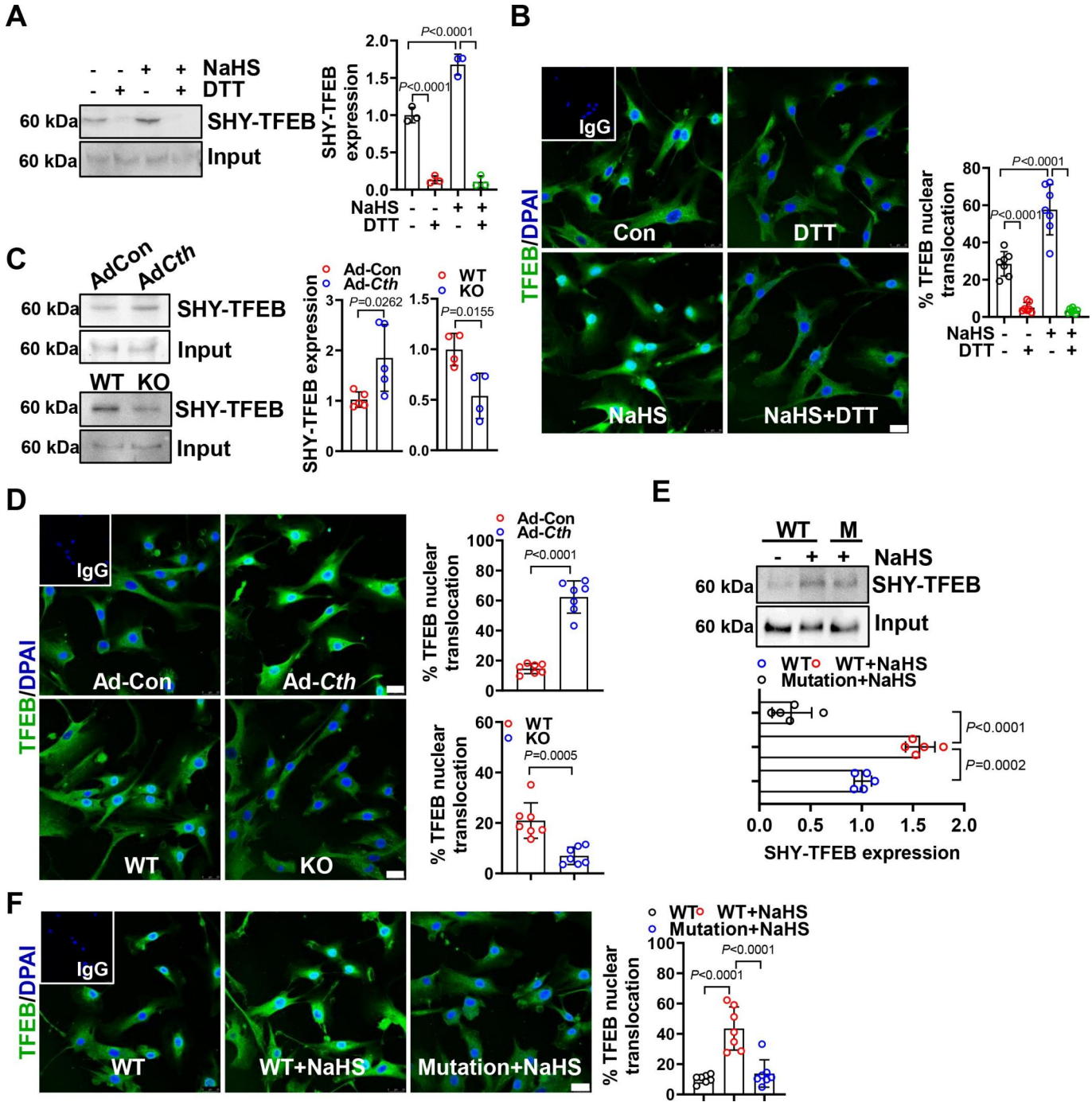

Figure 7. H_2S sulfhydrated TFEB and facilitated TFEB activity. Modified biotin switch assay measured sulfhydrated-TFEB (SHY-TFEB) (N = 3) (A). In HAMSCs, NaHS (100 μM, 2 h) increased but DTT (200 μM, 2 h) removed TFEB sulfhydration on its nuclear translocation. IgG as negative control, N = 7 (B). The effect of *Cth* overexpression by Ad*Cth* transfection (25 MOI, 24 h) (N = 5) or *cth* knockout (N = 4) on TFEB sulfhydration (C), association with TFEB nuclear translocation (D). N = 7, IgG as negative control. The C212S mutation TFEB plasmid (2 μg, 24 h) transfected into HASMCs, the NaHS-induced SHY-TFEB (N = 5) (E) and its nuclear translocation (N = 7) (F) were measured. IgG as negative control. All scale bar: 25 μm.

that these genes enriched in autophagy, response to acidic PH, calcium ion transport and lipid catabolic process (Figure 8D–E). Among these genes, we selected genes association with autophagosome (ATG9A), lysosome biogenesis (LAMP5) and cholesterol metabolism (LDLRAP1) for next analysis. Using integrative genomics viewer screenshots of selected genes tracks, we showed that TFEB C212S mutation (Figure 8F) and *cth* knockout (Figure 8G) decreased *TFEB* binding to the promoter of these genes. By Discriminative Regular Expression Motif Elicitation (Figure S8B) predicted the binding domain of *TFEB*, we analyzed the promoter of these genes and designed the primers, then validated these *TFEB* binding to occupancy genes downregulated by ChIP-qPCR (Figure S8C-D). NaHS enhanced the mRNA expression of *ATG9A*, *LAPTM5* and *LDLRAP1*, and which was reversed by *TFEB* knockdown (Figure 8H). On the contrary, PPG treatment reduced *ATG9A*, *LAPTM5* and *LDLRAP1* expression, which was reversed by WT p*TFEB* but not p$TFEB^{C212S}$ transfection

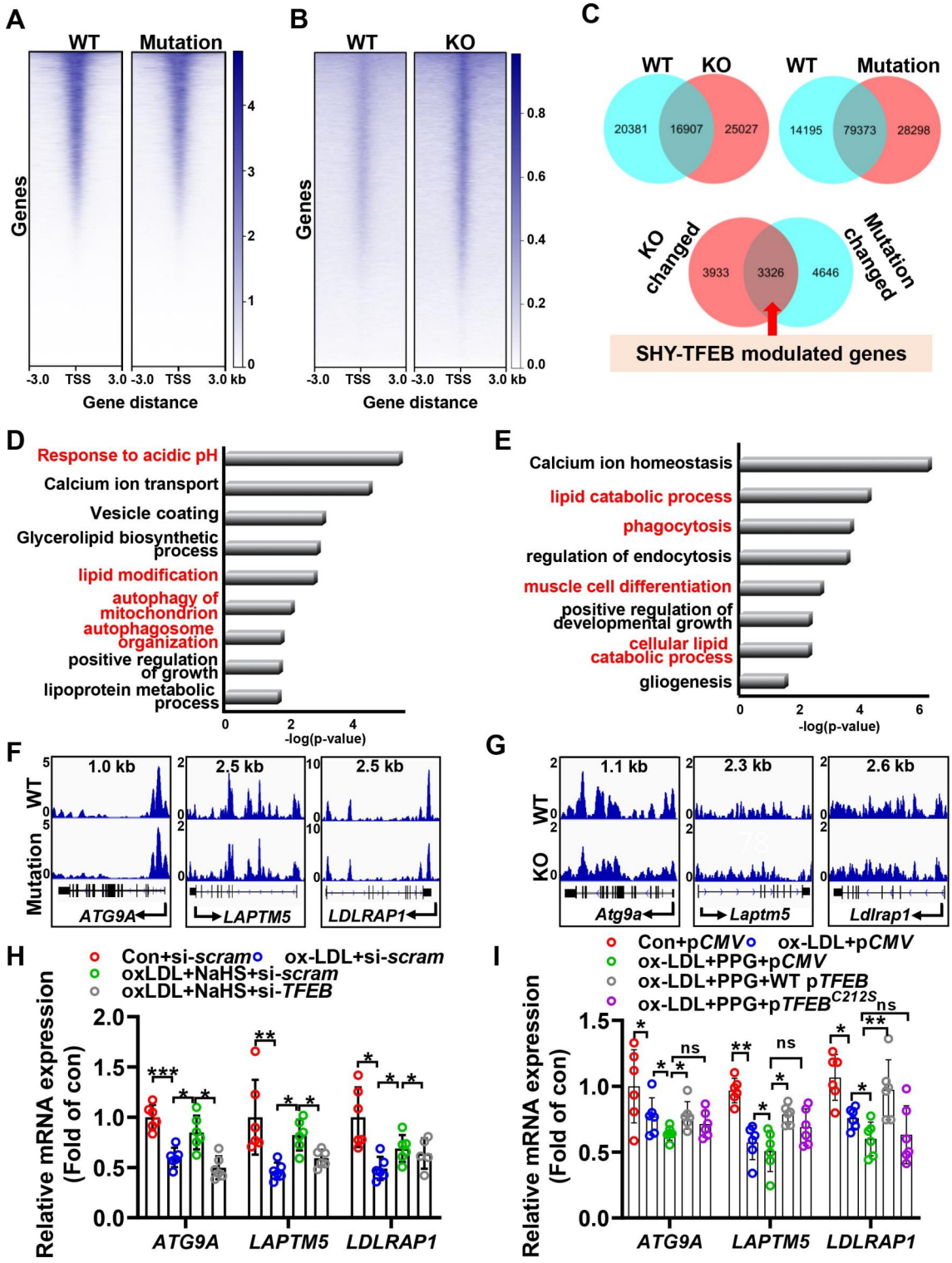

Figure 8. Sulfhydrated TFEB promoted autophagy, lysosome biogenesis and lipid metabolism related gene expression. Heat map of *TFEB*-occupied genes based on *TFEB* signal around *TFEB* peak center, in C212S mutation TFEB (could not be sulfhydrated) cells (A) and sulfhydrated TFEB reduced VSMCs (*cth* knockout) (B). Venn diagram to show peak numbers in different groups (upper panel), and modification sulfhydrated-TFEB (*cth* knockout and C121S mutation) changed genes, analysis overlapped genes suggesting conserved sulfhydrated-TFEB occupied genes (lower panel) (C). Gene Ontology (GO) analysis of sulfhydrated-TFEB target genes in C212 mutation cells (D) and *cth* knockout VSMCs (E). Visualization of ChIP-Seq results for three representative *TFEB* occupied genes (*ATG9A, LAPTM5* and *LDLRAP1*) by Integrative Genomics Viewer (IGV) in C212 mutation cells (F) and *cth* knockout VSMCs (G). Knockdown TFEB by siRNA transfection (100 nM, 24 h) effects on NaHS (100 μM, 2 h) modulating mRNA changes of *ATG9A, LAPTM5* and *LDLRAP1* in HASMCs. N = 6 (H). The effect of transfection WT or C212S mutation TFEB (2 μg, 24 h) on PPG-regulated mRNA levels of *ATG9A, LAPTM5* and *LDLRAP1* in 293A cells. N = 6 (I).

(Figure 8I), indicating that CTH induced these genes expression in an TFEB-dependent manner. Taken together, our data provide the direct evidence that sulfhydrates TFEB directly regulates autophagosome, lysosome biogenesis and cholesterol metabolism.

Discussion

The present study first identified that human intraplaque CTH level is closely correlated with plaque vulnerability (r = 0.9033). Furthermore, CTH-H_2S dramatically downregulated in intraplaque ACTA2-positive cells from patients, atherosclerotic mice, or ox-LDL–stimulated VSMCs. Deletion of *Cth* in VSMCs exacerbated size of plaque, lowered plaque stability due to the reduction of autophagy, all of which was partly rescued by H_2S donor supplementation. For the mechanism, we demonstrated that CTH-H_2S sulfhydrated TFEB to activate its transcription activity, modulating autophagosome formation, lysosome biogenesis, and cholesterol metabolism-related gene expression, then regulated autophagy procession and lysosome function.

Plaque stability tightly linked with cerebrovascular and cardiovascular events. Many studies addressed on the biomarkers for plaque stability such as microcalcification [20], inflammation [21], microRNAs [22]. More and more studies demonstrated that VSMCs function contributed to the plaque stability. VSMCs proliferation and migration per se promote the progress of plaque [23]. Conversely, VSMCs secreted extracellular matrix (COL1 and COL3) majorly contribution to the formation of fibrous cap [24]; but MMP2 (matrix metallopeptidase 2) and MMP9 degraded extracellular matrix, to promote VSMCs proliferation and migration and make fibrous cap thinner [25]. Of course, VSMC apoptosis, necrosis, senescence and autophagy attribute to plaque's progression and stability and well discussed in the reviews [4,5]. Here, we evaluated patient's intraplaque $CD68^+$ area, necrotic core area, $ACTA2^+$ area and collagen fraction thereby counting the vulnerable index, and demonstrated that intraplaque CTH protein level negatively correlated with vulnerable index. Surprisingly, the correlation coefficient is beyond 0.9 although it is just a small sample study. This is a very novel potential marker for plaque stability. How to define the cut values, how to transfer the clinical using need more works in the future.

Here, we found that CTH-H_2S was downregulated in VSMCs and VSMC-derived cells of human and mouse plaque, consistent with the changes in aortic tissues of the *apoe*$^{-/-}$ atherosclerotic mouse model [15]. As an essential foam-cell inducer, ox-LDL decreased CTH expression in human umbilical vein endothelium [26] or phosphorylated CTH at ser377 to reduce its enzyme activity [27], thus decreasing H_2S generation. Similarly, ox-LDL dose-dependently reduced *CTH* mRNA and protein expression and H_2S production in HASMCs. For the mechanism, ox-LDL induced DNA methylation in the promoter of *CTH* gene [28], and DNA demethylase-TET2 protected it [26]. Therefore, at least, the hypercholesterolemia impaired CTH-H_2S system causing the loss of H_2S protection in plaque progression.

Global knockout of *Cth* or *cth-apoe* double-knockout mice exacerbated atherosclerosis development [16]. By contrast, H_2S donor or overexpression of *Cth* has anti-atherogenesis effects [15,17,29]. CTH-H_2S is expressed in endothelium [30], and deletion of *Cth* in endothelium promoted plaque development and endothelial inflammation by lowering human antigen R sulfhydration [27]; however, H_2S sulfhydrated SIRT1 inhibited endothelial inflammation, then reduced atherosclerosis [18]. VSMCs are the largest component in the vascular wall; they play a critical role in atherosclerotic development and plaque stability [4]. VMSCs are also a major source of H_2S by CTH catalysis [31]. For pathophysiological relevance, knockout of *Cth* in VSMCs lost 75% of H_2S generation and exacerbated atherosclerosis progression, increased the necrotic core and reduced the fibrous cap of plaque, which was further confirmed by H_2S donor rescue. Our results first clarified the essential role of VSMC endogenous CTH-H_2S in plaque stability.

Autophagy is a process of clearing damaged organelles and proteins, maintaining intracellular metabolic homeostasis. Many studies demonstrate that H_2S is an activator of autophagy to play a protective role in endocrine, cardiovascular and other diseases [32]. H_2S activated multiple signal cascades such as PI3K-AKT-MTOR, AMPK-MTOR and STK11/LKB1-STRAD-CAB39/MO25, inducing autophagy to alleviate hepatic ischemia/reperfusion, nonalcoholic fatty liver disease and cancer [33–35]. In cardiovascular system, H_2S increased autophagy by the PI3K-AKT pathway reducing myocardial fibrosis [36]. Exogenous H_2S inhibited KEAP1 ubiquitination to induce autophagy-related protein expression, then exerted antioxidant effect on the cardiomyocytes of diabetic rats [37]. High glucose and palmitate induced rat aortic endothelial cells apoptosis. H_2S donor decreased mitochondrial fragments via MFN2 and provoked mitophagy to repress rat aortic endothelial cells apoptosis [38]. In line with previous study, we found that H_2S also plays a protect role in ox-LDL–induced VSMCs via provoking autophagy. Here, we firstly confirmed that VSMC autophagy was reduced in plaque of patients and mice, since of VSMC autophagy has a protective role in plaque stability [5]. VMSC-specific knockout of *Cth* further decreased autophagy and aggravated plaque vulnerability. In VMSC, high concentration of ox-LDL (>60 μg/ml) induced a foam cell-like phenotype and reduced autophagy [9]. Consistently, by loss- and gain-of-function experiments, we demonstrated that CTH-H_2S had anergic effects of ox-LDL. These findings support that *Cth* deficiency in VSMCs accelerated plaque vulnerability in part by mediating autophagy.

Autophagy is a lysosome-dependent process [39,40]. Here, we demonstrated that CTH-H_2S in VMSCs modulated autophagosome formation, autophagosome–lysosome fusion and lysosome degradation by using inhibitors and detecting lysosome pH value. For the mechanism, we investigated a core transcription factor, TFEB, a master regulator of lysosome biogenesis and autophagy [41]. TFEB has benefit for atherosclerosis by inhibiting endothelial inflammation [42], modulating VSMC proliferation and migration [43], and reducing foam-cell formation from VSMCs [44] and macrophages [45]. Here, we found that TFEB expression in ACTA2–positive cells were reduced in *cth*$^{SMC-/-}$ mice, which was rescued by H_2S donor treatment. In HASMCs, CTH-H_2S blocked the

effect of ox-LDL on TFEB expression, nuclear translocation and autophagy. In addition, H_2S or PPG actions on autophagy flux, collagen secretion and cell apoptosis were blocked by genomic interference of *TFEB*. These results indicate that CTH-H_2S activated VSMC autophagy then attenuated cell apoptosis and increased collagen secretion by modulating TFEB.

TFEB activity is mediated by post-translational modification [46,47]. MTORC1 can phosphorylate TFEB at serine 142 and 211, promote its binding to YWHA/14-3-3 protein and then inhibit its nuclear translocation [47,48]. Thus, H_2S inhibition of MTORC1 [49] might dephosphorylate TFEB, then enhance its activity. On the other hand, we identified a novel post-translational modification, sulfhydration, at the Cys212 site of TFEB. By pharmacological and genomic modification, we demonstrated that TFEB Cys212 sulfhydration enhanced its nuclear translocation; removal of sulfhydration or mutation of the Cys212 site decreased TFEB activity. Subsequently, ChIP-seq revealed that C212S mutation (removing sulfhydration) or lowered sulfhydration (*cth* knockout) reduced TFEB binding activity, then ChIP-qPCR confirmed 3 target genes, including *ATG9A* (autophagosome formation-related), *LAPTM5* (lysosome biogenesis) and *LDLRAP1* (LDL receptor cytoplasm tail binding protein, a gene of autosomal recessive hypercholesterolemia). On association with TFEB activation by H_2S, its own transcription was also upregulated by a self-feedback loop [50]. Thus, sulfhydration is a novel post-translational modification of TFEB for its activity and expression.

In conclusion, the present study revealed the essential role of VSMC endogenous CTH-H_2S in atherosclerotic development and plaque stability. On translational medicine aspect, some nanoprobe such as SPP1/osteopontin antibody-based nanoprobe could be used for noninvasive evaluation vulnerable plaque [51]; thus, CTH antibody-based probe might be also designed and used. For therapeutics, some H_2S-releasing donors such as SG1002 for heart failure are in phase I clinical trials [52], ATB-346 for anti-inflammation in a phase II clinical trial [53] showed some beneficial effects. Our work offers a further possibility of these drugs for atherosclerosis therapy and treating vulnerable plaque.

Materials and methods

Human atherosclerotic plaque samples

Human atherosclerotic plaque specimens were obtained from the 18 patients undergoing off-pump coronary artery bypass grafting-carotid endarterectomy surgery at the Department of Cardiovascular Surgery, Fuwai Hospital. The study was approved by Fuwai Hospital Ethics Committee and performed in accordance with the ethical standards. The patient clinical characteristics are summarized in Table S1. Tissue samples were used for immunofluorescence, immunohistochemistry or other staining.

Mice and atherosclerotic models

We generated VSMC-specific *cth* knockout mice by loxp-Cre system. All mice were inbred in a C57BL/6 background. Loxp sites flank exon 2 and exon 3 of the *Cth* gene. $Cth^{flox/flox}$ mice were crossed with *Tagln-Cre* mice to generate smooth muscle cell-specific *cth* knockout mice ($cth^{flox/flox}$-$Tagln^{Cre/+}$) and Cre recombinase negative littermates mice ($Cth^{flox/flox}$-$Tagln^{+/+}$) were used as controls. Age-matched littermate controls and condition knockout male mice were used for experiments. For atherosclerotic models [54], 8- to 10-weeks-old male mice were given a single tail vein injection of adeno-associated virus rAAV8-HCRApoE/hAAT-D377Y-mPCSK9 (5×10^{11} vector genome copies/injection diluted in 200 μl sterile saline solution) (WZBioscience Inc, AV208001-AV8). The atherosclerosis model design and execution complied with the guideline [55]. Following, mice were intraperitoneal injected with normal saline or NaHS (2 mg/kg bodyweight) (Sigma-Aldrich, 161,527) every day on Paigen diet (Shanghai Hongbai Technology Co., Ltd, D1209C) for 16 weeks. Animal were maintained under controlled temperature and a 12-h light/dark cycle with free access to water and diet. All animal protocols complied with all relevant ethical regulations and were approved by the Institutional Animal Care and Use Committee, the Experimental Animal Center, Fuwai Hospital, National Center for Cardiovascular Diseases, China.

Immunofluorescence and immunohistochemical staining

For immunofluorescence staining, VSMCs, aortic root, aorta frozen sections or cells were fixed with 4% paraformaldehyde (Solarbio, P1110) for 15 min, permeabilized with 0.1% Triton X-100 (Sigma-Aldrich, 9002–93-1) in PBS (Sigma-Aldrich, 806,552), rinsed, incubated in 0.5% BSA (Sigma-Aldrich, V900933) in PBS for 30 min, and then aortas were incubated with specific primary antibody at 4°C overnight in incubation buffer containing 1% BSA. Primary antibodies were used as follows: anti-ACTA2 (Abcam, ab7817), anti-TFEB (Abcam, ab2636) or anti-LC3B (Abcam, ab48394). After washing 3 times with PBS, slices were incubated with Alexa Fluor 488- (Abcam, 150,077) or Alexa Fluor 594- conjugated secondary antibodies (Abcam, ab150116) for 1 h at room temperature. Fluorescent signals were detected using Leica confocal laser scanning microscopy.

For immunohistochemistry staining, human and mice plaques paraffin sections were dewaxed with xylene (Sango Biotech, A530011-0500) and ethanol (InnoChem Technology, A60719) before rehydration. Then, slices infiltrated into 3% H_2O_2 (Lovibond, ET512380) to quench endogenous peroxidase, then transferred into heat sodium citrate buffer (95°C) by pressure cooker. After 5 min, the slides were blocked in 1% BSA for 30 min at 37°C and incubated with primary antibodies against CD68 (Abcam, ab955) and ACTA2 (Abcam, ab7817) overnight at 4°C. The next day, HRP-conjugated secondary antibodies (Gene-Protein Link, P03S02L and P03S01) were added. After developing the

color by incubation with diaminobenzidine, slices were counterstained with hematoxylin (Beyotime, C0107).

Vulnerability index

Vulnerability index was calculated as reported previously [56]. Briefly, Vulnerability index = Unstable parameter/stable parameters. Unstable parameters are the sum of $CD68^+$ area plus necrotic core area; stable parameters are the sum of $ACTA2^+$ area and collagen volume.

Atherosclerotic lesion analysis

For quantification of atherosclerotic lesion, Oil Red O (Sigma-Aldrich, 01018)-positive lesion surface areas on en face preparation of whole aorta were measured. Briefly, aorta from root to the abdominal area was dissected and fixed with formalin, and followed by removing the connective tissues carefully. Then, the entire aorta was opened longitudinally, pinned en face, stained with Oil Red O, and photographed with digital camera. Atherosclerosis lesion at the aortic root was studied in tissue cross-sections. The base of the heart including the most proximal part of the ascending aorta was excised and embedded in O. C.T. compound (SAKURA, 4583). The tissue piece was oriented to have all three aortic valves in the same geometric plane. The portion containing the aortic root was cut consecutively into 8 μm sections, starting from the commissures of the aortic cusps. To assess the atherosclerotic lesion, necrotic core and fibrosis cap, sections were stained with Oil red O, H&E staining (Beyotime, C0105S) and Masson (LEAGENE, DC0032). The stained specimens were evaluated by light microscopy.

Cellular H_2S product assay.

To measure intracellular H_2S levels, HASMCs cells were treated with ox-LDL (Yiyuan Biotechnologies, YB002) for 2 h, then washed three times with PBS. 10 μM synthesized mito-HS (H_2S fluorescence probe) was added and cells were continuously cultured for 1 h in a dark box in a CO_2 incubator [57]. Fluorescence images were acquired by confocal microscopy.

Quantification of lipid levels

Blood samples were collected into heparin-coated tubes. The samples were centrifuged at 3,000 x g for 15 min to obtain plasma that was used for determination. Total plasma cholesterol (CHO) (BioSino, 000180), triglycerides (TGs) (BioSino, 000220), low density lipoprotein cholesterol (LDL-C) (BioSino, 020245), and high-density lipoprotein cholesterol (HDL-C) levels (BioSino, 020235) were determined using assay kits.

For cellular lipid deposition, cells were staining with HCS LipidTOX (Invitrogen, H34476). Images were scanned by Leica confocal laser scanning microscopy; positive spot area statistics was performed by using the Opera Phenix High-Content Screening System and Harmony software from Perkin Elmer.

Primary mouse VSMCs isolation

Male mice (5- to 6-weeks old) were anesthetized and whole aortas were quickly dissected. After removal of adventitial connective tissues and luminal endothelial cells, the aortas were cut into pieces of approximate 1 mm^2 and digested in 10 mL of Dulbecco's modified Eagle's medium (DMEM; Thermo Fisher Scientific, C11995500BT) containing 1 mg/mL collagenase II (Thermo Fisher Scientific, 17,101–015) for 4 h at 37°C. The VSMCs were collected by centrifuge at 800 x g for 10 min. Cells were resuspended with DMEM and planted in 10-cm dish for culturing. Medium was changed every 2 days, and cells at passages 3 to 8 were used.

Cell culture and treatment

Human aortic smooth muscle cells (HASMCs) were purchased from ScienCell (6110), HASMCs cultured with smooth muscle cell medium (ScienCell, 1101) containing 2% fetal bovine serum. Primary mouse VSMCs were cultured in Dulbecco's modified Eagle's medium containing 10% fetal bovine serum. All cells were cultured and maintained at 37°C and 5% CO_2. For cell treatment, NaHS (Sigma-Aldrich, 161,527), PPG (Sigma-Aldrich, P7888), 3-MA (Sigma-Aldrich, M9218) and CQ (Sigma-Aldrich, H0915) were used in this study. Cells were treated with NaHS (100 μM, 2 h) or PPG (100 μM, 24 h). For determining the effect of autophagy inhibitor, cells were pre-treated with 5 mM 3-MA for 1 h or treated with 200 μM CQ for 2 h.

Cell apoptosis analysis

Cell apoptosis was detected by FITC AnnexinV apoptosis detection kit (BD Biosciences, 556,547). Briefly, cells were washed with cold PBS twice and resuspend cells in 1× binding buffer, and then added 5 μl FITC-ANXA5/annexin V and 5 μl propidium iodide to every tube. After 15-min incubation at room temperature in the dark, cells were analyzed by flow cytometry.

Transfection

siRNA and scrambled siRNA-negative control were synthesized by Biolino biotechnologies lnc (Beijing, China). The si-*TFEB* sequences are as follows: sense 5'-GGAGGACGCAGUGAACAUATT-3'; antisense 5'-UAUGUUCACUGCGUCCUC- CTT-3'. For transient transfection, cell lines were seeded at 60% confluency. Transfection experiments were performed with 100 nM siRNA or 2 μg TFEB plasmid (ORIGENE, RC207153) using Lipofectamine 3000 (Invitrogen, L3000015) according to the manufacturer's guidelines. *Cth* overexpressed and sh*Cth* adenovirus were constructed by WZBioscience (Shandong, China). 25 MOI was used for 24 h.

Autophagy flux determination

For detecting autophagy flux, mRFP-GFP-LC3 adenovirus (HanBio, HB-AP2100001) was used. VSMCs were transfected with mRFP-GFP-LC3 (25 MOI) for 24 h. The fresh complete medium was changed and cells were viewed under a fluorescence microscope. For image requirement, the GFP and mRFP dots was scanned by Leica confocal laser scanning microscopy. Statistical analysis was performed by the Opera Phenix High-Content Screening System and Harmony software (Perkin Elmer).

Lysosomal pH determination

Lysosomal pH was detected by using LysoSensor Yellow/Blue DND-160 (Invitrogen, L7545). In brief, cells were labeled with 3 mmol/L LysoSensor Yellow/Blue DND-160 in culture medium at 37°C for 5 min. After washing twice with cold PBS, immediately analyzed by using a microplate reader (excitation, 360 nm; emission, 451 and 518 nm). Quantification of lysosomal pH involved a ratio (emission 451:emission 518) according to pH calibration.

Transmission electron microscopy

Aorta was cut into small pieces about 1 cm^2 and then immersed in 2.5% glutaraldehyde-PBS overnight. For treatment, cells were washed with PBS 3 times after digestion, and the supernatant discarded. 2.5% glutaraldehyde was added in the pellet. After washing with 0.1 M imidazole buffer, tissue pieces were post-fixed with 1% osmium tetroxide in 0.1 M imidazole buffer at 4°C, dehydrated through a graded series of ethanol solutions, rinsed in propylene oxide (InnoChem Technology, A36774), and embedded in epoxy resin (Santa Cruz, sc-214,554). Ultra-thin sections (50 nm) were prepared and stained with 1% uranyl acetate (SERVA, 7,787,002) and 0.25% lead citrate (BioRuler, RH109410). Finally, these sections were examined and visualized under a transmission electron microscope. To quantify autophagosomes, four micrographs were taken with systematic random sampling from each sample and taken the average. For each experimental group, at least six samples were counted. The number of autophagosomes were counted from each micrograph manually by three investigators.

Nuclear/cytosol fractionation

Nuclear and cytosol fractionation isolation is finished by assay kit (APPLYGEN, P1200). When cells reach 90% confluence, detach the cells by tyrosinase. Collected and centrifuged the cells. Cytosol extraction buffer was added in packed cell. After incubation and centrifugation, the supernatant was cytosol extract. Added cold nuclear extraction buffer into the pellet containing crude nuclei, the supernatant fraction contains the proteins extracted from nuclear after centrifugation. The nuclear and cytosol were resuspended in SDS sample buffer, and the fractions were subjected to Western blot analysis.

Biotin switch assay

The assay was performed as described with modification [18]. Briefly, VSMCs treated with H_2S or DTT (Sigma-Aldrich, 10,197,777,001), then homogenized in RIPA lysis buffer (Sigma-Aldrich, USA). The homogenates were centrifuged at 14,000 x g (4°C) for 15 min. The supernatant was collected and protein was quantified by BCA assay (Thermo Fisher Scientific, 23,227). Primary anti-TFEB antibody (2 μg) was added into the protein lysis (1 mg/mL) containing protein G beads (Invitrogen, 10004D) and rotated incubation overnight at 4°C. Beads were washed with PBS 3 times, then blocked with HEN buffer (containing 2.5% SDS [Beyotime, ST626] and 20 mM methyl methanethiosulfonate [MMTS; BioRuler, RH102923]) at 50°C for 20 min. MMTS was removed by precipitating proteins with acetone (Sigma-Aldrich, 904,082) at – 20°C for 20 min. After acetone removal, protein was resuspended in HENS buffer (containing 1% SDS), and 4 mM biotin-HPDP (LDBIO, 2329–250) was added for incubation for 4 h at room temperature. Biotinylated-protein was pulled down by streptavidin magnet beads (Beyotime, P2151) and eluted by SDS-PAGE loading buffer and subjected to Western blot analysis.

Western blot analysis

Cells were extracted in RIPA buffer (Solarbio, R001) supplemented with complete protease inhibitor cocktail (Thermo Fisher Scientific, TF267510). Protein (40 μg) was separated on SDS-PAGE and transferred into nitrocellulose membrane (Pall Corporation, 66,485). Membrane was blocked, then incubated in the presence of specific primary antibodies at 4°C overnight. Matching secondary horseradish peroxidase (HRP)-conjugated IgG was applied and immunoreactive protein bands were detected using Western blot luminol reagent (Merck, WBKLS0500). Antibodies used included anti-TFEB (Abcam, ab2636), anti-LC3B (Abcam, ab48394), anti-LAMP1 (Abcam, ab24170), anti-SQSTM1/p62 (Abcam, ab56416), anti-CTH (Proteintech, 60,234-1-lg), anti-ACTB (Abcam, ab8227) and anti-GAPDH (Abcam, ab75423).

RNA isolation and quantitative real-time polymerase chain reaction

Total RNAs were isolated using Trizol (Thermo Fisher Scientific, 15,596,018) according to the manufacturer's instructions. A total of 2 μg of RNA was reverse-transcribed into cDNA. Following reverse transcription (Invitrogen, K1622), qRT-PCR was performed using SYBR Green PCR master mix (YEASEN, 11202ES08) on an ABI 7300 Sequence Detection System with the following conditions: 50°C for 2 min and then at 95°C for 10 min, followed by 40 cycles of amplification (95°C for 15s; 60°C for 30s; 80°C for 30s). GAPDH was used as the endogenous normalizer. The primers used were listed in Table S2.

Chromatin immunoprecipitation sequencing (ChIP-seq)

ChIP assays were performed using chromatin immunoprecipitation kit (Merck, 17–10,086). Cells were cross-linked to final 1% formaldehyde for 10 min, followed by quenching with 125 mM glycine for 5 min at room temperature, and by washing with tris-buffered saline (TBS; Gene-Protein Link, P05B03). The pellets were resuspended in cell lysis buffer (10 mM Tris-HCl, pH 7.5, 10 mM NaCl, 0.5% NP-40 [Solarbio, N8031]) and incubated on ice for 10 min. Cross-linked chromatin was sonicated into 200-bp to 500-bp fragments. After centrifuging, the clean supernatant was incubated with 4 μg of anti-TFEB antibody overnight at 4°C. Beads were washed extensively with ChIP buffer, high-salt buffer, $LiCl_2$ buffer and TE buffer. Bound chromatin was eluted and reverse-crosslinked at 65°C overnight. DNA was recovered by RNase A and proteinase K treatment, phenol-chloroform extraction and ethanol precipitation. Then the DNA was purified using spin columns. After preparing ChIP library, the size and quality of the DNA was confirmed by Aglient 2100 bioanalyzer. Then the ChIP library were sequenced on an Illumina NextSeq 500 sequencers. Enrichment was confirmed by targeted real-time PCR in positive genomic loci. The primer sequences are listed in Table S3.

For analysis of ChIP-seq results, Raw reads were filtered to obtain high-quality clean reads by removing sequencing adapters, short reads (length <50 bp) and low-quality reads using Cutadapt (v1.9.1) and Trimmomatic (v0.35). Then FastQC is used to ensure high reads quality. The clean reads were mapped to the mouse genome (assembly GRCm38.p6) using the Bowtie2 (v2.2.6) software. Peak detection was performed using the MACS (v2.1.1) peak finding algorithm with 0.01 set as the p-value cutoff. Annotation of peak sites to gene features was performed using the ChIPseeker R package. For functional enrichment analysis, gene annotation file was retrieved from Ensembl genome browser databases (http://www.ensembl.org/index.html). To annotate genes with gene ontology (GO) terms, ClusterProfiler (R package) was used.

Statistical analysis

Data are presented as mean with standard deviation (SD). Differences between two groups were evaluated with unpaired Student's t-test. For three or more groups, data were compared by one-way ANOVA followed by Tukey post-hoc analysis. Comparisons including two factors were performed by two-way ANOVA. Repeated measures on the same animals were analyzed using two-way mixed-effects ANOVA. All statistical analysis involved using GraphPad Prism v8.0.2. $P < 0.05$ was considered statistically significant.

Acknowledgments

We thank Prof. Jichun Yang from Peking University Health Science Centre for providing technical assistance of primary mouse VSMCs isolation. We thank Prof. Xinjing Tang from Peking University Health Science Centre for synthesising and providing mito-HS.

Disclosure statement

No potential conflict of interest was reported by the author(s).

Funding

This work was supported by the Chinese Academy of Medical Sciences Innovation Fund for Medical Sciences [2021-I2M-1-007]; National Natural Science Foundation of China [81800367]; National Natural Science Foundation of China [81825002]; National Natural Science Foundation of China [81870318]; National Key R&D Program of China [2018YFC1312703]; Beijing Outstanding Young Scientist Program [BJJWZYJH01201910023029].

Abbreviations

ATG9A: autophagy related 9A; CTH: cystathionine gamma-lyase; CQ: chloroquine; HASMCs: human aortic smooth muscle cells; H_2S: hydrogen sulfide; LAMP1: lysosomal associated membrane protein 1; LAPTM5: lysosomal protein transmembrane 5; NaHS: sodium hydrosulfide hydrate; ox-LDL: oxidized-low density lipoprotein; PPG: DL-propagylglycine; TFEB: transcription factor EB; 3-MA: 3-methyladenine; VSMCs: vascular smooth muscle cells.

ORCID

Zhenzhen Chen http://orcid.org/0000-0001-9919-3997
Chenxi Ouyang http://orcid.org/0000-0002-3283-3141
Haizeng Zhang http://orcid.org/0000-0002-1500-9265
Yuanrui Gu http://orcid.org/0000-0002-8750-3078
Yue Deng http://orcid.org/0000-0001-9717-9163
Congkuo Du http://orcid.org/0000-0001-9865-3883
Changting Cui http://orcid.org/0000-0002-5056-3608
Shuangyue Li http://orcid.org/0000-0002-7843-8630
Wenjie Wang http://orcid.org/0000-0003-4179-4137
Wei Kong http://orcid.org/0000-0001-6720-6810
Jingzhou Chen http://orcid.org/0000-0002-1642-003X
Jun Cai http://orcid.org/0000-0002-8928-9570
Bin Geng http://orcid.org/0000-0001-7573-8710

References

[1] Lu H, Daugherty A. Atherosclerosis. Arterioscler Thromb Vasc Biol. 2015 Mar;35(3):485–491.
[2] Bennett MR, Sinha S, Owens GK. Vascular smooth muscle cells in atherosclerosis. Circ Res. 2016 Feb 19;118(4):692–702.
[3] Allahverdian S, Chaabane C, Boukais K, et al. Smooth muscle cell fate and plasticity in atherosclerosis. Cardiovasc Res. 2018 Mar 15;114(4):540–550.
[4] Grootaert MOJ, Moulis M, Roth L, et al. Vascular smooth muscle cell death, autophagy and senescence in atherosclerosis. Cardiovasc Res. 2018 Mar 15;114(4):622–634.
[5] Basatemur GL, Jorgensen HF, Clarke MCH, et al. Vascular smooth muscle cells in atherosclerosis. Nat Rev Cardiol. 2019 Dec;16(12):727–744.
[6] Perrotta I. The use of electron microscopy for the detection of autophagy in human atherosclerosis. Micron. 2013 Jul;50:7–13.
[7] Kockx MM, De Meyer GR, Muhring J, et al. Apoptosis and related proteins in different stages of human atherosclerotic plaques. Circulation. 1998 Jun 16;97(23):2307–2315.
[8] Michiels CF, Fransen P, De Munck DG, et al. Defective autophagy in vascular smooth muscle cells alters contractility and Ca(2)(+) homeostasis in mice. Am J Physiol Heart Circ Physiol. 2015 Mar 15;308(6):H557–67.
[9] Ding Z, Wang X, Schnackenberg L, et al. Regulation of autophagy and apoptosis in response to ox-LDL in vascular smooth muscle cells, and the modulatory effects of the microRNA hsa-let-7 g. Int J Cardiol. 2013 Sep 30;168(2):1378–1385.

[10] Dai XY, Zhao MM, Cai Y, et al. Phosphate-induced autophagy counteracts vascular calcification by reducing matrix vesicle release. Kidney Int. 2013 Jun;83(6):1042–1051.
[11] Osonoi Y, Mita T, Azuma K, et al. Defective autophagy in vascular smooth muscle cells enhances cell death and atherosclerosis. Autophagy. 2018;14(11):1991–2006.
[12] Luo Z, Xu W, Ma S, et al. Moderate autophagy inhibits vascular smooth muscle cell senescence to stabilize progressed atherosclerotic plaque via the mTORC1/ULK1/ATG13 signal pathway. Oxid Med Cell Longev. 2017;2017:3018190.
[13] Michiels CF, Kurdi A, Timmermans JP, et al. Spermidine reduces lipid accumulation and necrotic core formation in atherosclerotic plaques via induction of autophagy. Atherosclerosis. 2016 Aug;251:319–327.
[14] Zhang Y, Tang ZH, Ren Z, et al. Hydrogen sulfide, the next potent preventive and therapeutic agent in aging and age-associated diseases. Mol Cell Biol. 2013 Mar;33(6):1104–1113.
[15] Wang Y, Zhao X, Jin H, et al. Role of hydrogen sulfide in the development of atherosclerotic lesions in apolipoprotein E knockout mice. Arterioscler Thromb Vasc Biol. 2009 Feb;29(2):173–179.
[16] Mani S, Li H, Untereiner A, et al. Decreased endogenous production of hydrogen sulfide accelerates atherosclerosis. Circulation. 2013 Jun 25;127(25):2523–2534.
[17] Liu Z, Han Y, Li L, et al. The hydrogen sulfide donor, GYY4137, exhibits anti-atherosclerotic activity in high fat fed apolipoprotein E(-/-) mice. Br J Pharmacol. 2013 Aug;169 (8):1795–1809.
[18] Du C, Lin X, Xu W, et al. Sulfhydrated sirtuin-1 increasing its deacetylation activity is an essential epigenetics mechanism of anti-atherogenesis by hydrogen sulfide. Antioxid Redox Signal. 2019 Jan 10;30(2):184–197.
[19] Qiu X, Liu K, Xiao L, et al. Alpha-lipoic acid regulates the autophagy of vascular smooth muscle cells in diabetes by elevating hydrogen sulfide level. Biochim Biophys Acta Mol Basis Dis. 2018 Nov;1864(11):3723–3738.
[20] Vancheri F, Longo G, Vancheri S, et al. Coronary artery microcalcification: imaging and clinical implications. Diagnostics (Basel). 2019 Sep 23;9(4). DOI:10.3390/diagnostics9040125.
[21] Poredos P, Gregoric ID, Jezovnik MK. Inflammation of carotid plaques and risk of cerebrovascular events. Ann Transl Med. 2020 Oct;8(19):1281.
[22] Solly EL, Dimasi CG, Bursill CA, et al. MicroRNAs as therapeutic targets and clinical biomarkers in atherosclerosis. J Clin Med. 2019 Dec 13;8(12):2199.
[23] Stegemann JP, Hong H, Nerem RM. Mechanical, biochemical, and extracellular matrix effects on vascular smooth muscle cell phenotype. J Appl Physiol. 1985 2005 Jun;98(6):2321–2327.
[24] Lusis AJ. Atherosclerosis. Nature. 2000 Sep 14;407(6801):233–241.
[25] Mason DP, Kenagy RD, Hasenstab D, et al. Matrix metalloproteinase-9 overexpression enhances vascular smooth muscle cell migration and alters remodeling in the injured rat carotid artery. Circ Res. 1999 Dec 3-17;85(12):1179–1185.
[26] Peng J, Tang ZH, Ren Z, et al. TET2 protects against oxLDL-Induced HUVEC dysfunction by upregulating the CSE/H2S system. Front Pharmacol. 2017;8:486.
[27] Bibli SI, Hu J, Sigala F, et al. Cystathionine gamma lyase sulfhydrates the RNA binding protein human antigen R to PRESERVE ENDOTHELIAL CELL FUNCTION AND DELAY ATHEROGENESIS. Circulation. 2019 Jan 2;139 (1):101–114.
[28] Du HP, Li J, You SJ, et al. DNA methylation in cystathionine-gamma-lyase (CSE) gene promoter induced by ox-LDL in macrophages and in apoE knockout mice. Biochem Biophys Res Commun. 2016 Jan 15;469(3):776–782.
[29] Cheung SH, Kwok WK, To KF, et al. Anti-atherogenic effect of hydrogen sulfide by over-expression of cystathionine gamma-lyase (CSE) gene. PLoS One. 2014;9(11):e113038.
[30] Yang G, Wu L, Jiang B, et al. H2S as a physiologic vasorelaxant: hypertension in mice with deletion of cystathionine gamma-lyase. Science. 2008 Oct 24;322(5901):587–590.
[31] Zhao W, Zhang J, Lu Y, et al. The vasorelaxant effect of H(2)S as a novel endogenous gaseous K(ATP) channel opener. EMBO J. 2001 Nov 1;20(21):6008–6016.
[32] Wang J, Wu D, Wang H. Hydrogen sulfide plays an important protective role by influencing autophagy in diseases. Physiol Res. 2019 Jun 30;68(3):335–345.
[33] Wu D, Wang H, Teng T, et al. Hydrogen sulfide and autophagy: a double edged sword. Pharmacol Res. 2018 May;131:120–127.
[34] Wang SS, Chen YH, Chen N, et al. Hydrogen sulfide promotes autophagy of hepatocellular carcinoma cells through the PI3K/Akt/mTOR signaling pathway. Cell Death Dis. 2017 Mar 23;8(3):e2688.
[35] Kundu S, Pushpakumar S, Khundmiri SJ, et al. Hydrogen sulfide mitigates hyperglycemic remodeling via liver kinase B1-adenosine monophosphate-activated protein kinase signaling. Biochim Biophys Acta. 2014 Dec;1843(12):2816–2826.
[36] Liu M, Li Z, Liang B, et al. Hydrogen sulfide ameliorates rat myocardial fibrosis induced by thyroxine through PI3K/AKT signaling pathway. Endocr J. 2018 Jul 28;65(7):769–781.
[37] Wu J, Tian Z, Sun Y, et al. Exogenous H2S facilitating ubiquitin aggregates clearance via autophagy attenuates type 2 diabetes-induced cardiomyopathy. Cell Death Dis. 2017 Aug 10;8(8):e2992.
[38] Liu N, Wu J, Zhang L, et al. Hydrogen sulphide modulating mitochondrial morphology to promote mitophagy in endothelial cells under high-glucose and high-palmitate. J Cell Mol Med. 2017 Dec;21(12):3190–3203.
[39] Jaishy B, Abel ED. Lipids, lysosomes, and autophagy. J Lipid Res. 2016 Sep;57(9):1619–1635.
[40] Mizushima N. Autophagy: process and function. Genes Dev. 2007 Nov 15;21(22):2861–2873.
[41] Settembre C, Di Malta C, Polito VA, et al. TFEB links autophagy to lysosomal biogenesis. Science. 2011 Jun 17;332 (6036):1429–1433.
[42] Lu H, Fan Y, Qiao C, et al. TFEB inhibits endothelial cell inflammation and reduces atherosclerosis. Sci Signal. 2017 Jan 31;10 (464). DOI:10.1126/scisignal.aah4214.
[43] Wang YT, Chen J, Li X, et al. Contribution of transcription factor EB to adipoRon-induced inhibition of arterial smooth muscle cell proliferation and migration. Am J Physiol Cell Physiol. 2019 Nov 1;317(5):C1034–C1047.
[44] Pi H, Wang Z, Liu M, et al. SCD1 activation impedes foam cell formation by inducing lipophagy in oxLDL-treated human vascular smooth muscle cells. J Cell Mol Med. 2019 Aug;23 (8):5259–5269.
[45] Sergin I, Evans TD, Zhang X, et al. Exploiting macrophage autophagy-lysosomal biogenesis as a therapy for atherosclerosis. Nat Commun. 2017 Jun 7;8(1):15750.
[46] Miller AJ, Levy C, Davis IJ, et al. Sumoylation of MITF and its related family members TFE3 and TFEB. J Biol Chem. 2005 Jan 7;280(1):146–155.
[47] Napolitano G, Ballabio A. TFEB at a glance. J Cell Sci. 2016 Jul 1;129(13):2475–2481.
[48] Napolitano G, Esposito A, Choi H, et al. mTOR-dependent phosphorylation controls TFEB nuclear export. Nat Commun. 2018 Aug 17;9(1):3312.
[49] Chen J, Gao J, Sun W, et al. Involvement of exogenous H2S in recovery of cardioprotection from ischemic post-conditioning via increase of autophagy in the aged hearts. Int J Cardiol. 2016 Oct 1;220:681–692.
[50] Settembre C, De Cegli R, Mansueto G, et al. TFEB controls cellular lipid metabolism through a starvation-induced autoregulatory loop. Nat Cell Biol. 2013 Jun;15(6):647–658.
[51] Ge X, Cui H, Kong J, et al. A non-invasive nanoprobe for in vivo photoacoustic imaging of vulnerable atherosclerotic plaque. Adv Mater. 2020 Sep;32(38):e2000037.
[52] Li Z, Polhemus DJ, Lefer DJ. Evolution of hydrogen sulfide therapeutics to treat cardiovascular disease. Circ Res. 2018 Aug 17;123(5):590–600.
[53] Wallace JL, Nagy P, Feener TD, et al. A proof-of-concept, phase 2 clinical trial of the gastrointestinal safety of a hydrogen

sulfide-releasing anti-inflammatory drug. Br J Pharmacol. 2020 Feb;177(4):769–777.
[54] Bjorklund MM, Hollensen AK, Hagensen MK, et al. Induction of atherosclerosis in mice and hamsters without germline genetic engineering. Circ Res. 2014 May 23;114(11):1684–1689.
[55] Daugherty A, Tall AR, Daemen M, et al. Recommendation on design, execution, and reporting of animal atherosclerosis studies: a scientific statement from the American Heart Association. Circ Res. 2017 Sep 1;121(6):e53–e79.
[56] Shami A, Atzler D, Bosmans LA, et al. Glucocorticoid-induced tumour necrosis factor receptor family-related protein (GITR) drives atherosclerosis in mice and is associated with an unstable plaque phenotype and cerebrovascular events in humans. Eur Heart J. 2020 Aug 14;41(31):2938–2948.
[57] Wu Z, Liang D, Tang X. Visualizing hydrogen sulfide in mitochondria and lysosome of living cells and in tumors of living mice with positively charged fluorescent chemosensors. Anal Chem. 2016 Sep 20;88(18):9213–9218.